Hopfion-Driven Magnonic Hall Effect and Magnonic Focusing

Carlos Saji,[1,2] Roberto E. Troncoso,[3] Vagson L. Carvalho-Santos,[4,2] Dora Altbir,[2,5,6] and Alvaro S. Nunez[1,2]
[1]Departamento de Física, FCFM, Universidad de Chile, Santiago 8370449, Chile
[2]Centro de Nanociencia y Nanotecnología CEDENNA, Avda. Ecuador 3493, Santiago, Chile
[3]School of Engineering and Sciences, Universidad Adolfo Ibáñez, Av. Diag. Las Torres 2640, 7941169 Santiago, Chile
[4]Departamento de Física, Universidade Federal de Viçosa 36570-900, Viçosa, Brazil
[5]Departamento de Física, Universidad de Santiago de Chile (USACH), CEDENNA, Avda. Ecuador 3493, 9170124, Santiago, Chile
[6]Universidad Diego Portales, Ejército 441, 8370179 Santiago, Chile

(Received 24 February 2023; revised 12 June 2023; accepted 13 September 2023; published 18 October 2023)

Hopfions are localized and topologically nontrivial magnetic configurations that have received considerable attention in recent years. In this Letter, we use a micromagnetic approach to analyze the scattering of spin waves (SWs) by magnetic hopfions. Our results evidence that SWs experience an electromagnetic field generated by the hopfion and sharing its topological properties. In addition, SWs propagating along the hopfion symmetry axis are deflected by the magnetic texture, which acts as a convergent or divergent lens, depending on the SWs' propagation direction. Assuming that SWs propagate along the plane perpendicular to the symmetry axis, the scattering is closely related to the Aharonov-Bohm effect, allowing us to identify the magnetic hopfion as a scattering center.

DOI: 10.1103/PhysRevLett.131.166702

Introduction.—The emergence of particlelike states on different systems [1,2] is at the crossroads of several fields in modern physics. From early classical mechanical models [3] to contemporary studies of elementary particles [4], the nature of such states remains a fertile ground where theorists and experimentalists converge. Such endeavors rely on the notion that some particle states are protected by their topology [5]. Regarding magnetic systems, in addition to the fundamental interest that topological protection offers, the potential for using magnetic quasiparticles in data processing and storage devices [6] draws attention from the applied point of view. Therefore, magnetic solitonic states, such as domain walls [7–10], vortices, and skyrmions [11–17], are relevant for current research in modern magnetism.

The possibility of controlling the size and shape of nanostructures allows the nucleation, stabilization, and control of three-dimensional (3D) magnetic patterns [18–21]. Among 3D textures, we can highlight the hopfion, which consists of a soliton in which the magnetization field swirls in a knotted pattern, creating a stable structure, as shown in Fig. 1. Magnetic hopfions have been theoretically studied for more than 20 years [22,23] focusing on their nucleation and stabilization processes [24–28], while their observation has been reported just recently [29].

In parallel, and due to their properties [30–33] and localized nature, spin waves (SWs) have been deeply analyzed, establishing their importance for spintronic devices. In this context, the interaction between SWs and magnetic textures is also a well-established research topic [34]. Among the essential phenomena displayed by such interaction, perhaps the most baffling one is the ability of SWs to change the momentum of a magnetic texture [35], inducing its motion. Another interesting fact related to

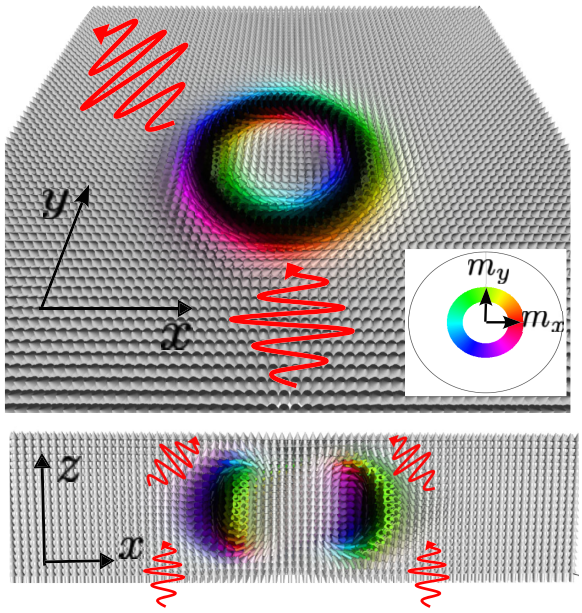

FIG. 1. Normalized magnetization $\boldsymbol{n}$ of a hopfion determined by the set of parameters given in the text. Top panel: cross section in the xy plane. Bottom panel: cross section in the xz plane. The color code represents the $\boldsymbol{n}$ projection along the xy plane. The red wavy lines represent the SWs-hopfion interaction. SWs propagating along the xy plane suffer skew-scattering, while SWs moving along the symmetry axis of the Hopfion are deflected similarly to a converging lens.

the interaction between SWs and topological magnetic objects, such as skyrmions [36], is the emergent magnetic field that can induce a magnon Hall effect. Additionally, magnonic bands in skyrmion crystals display a topological structure in momentum space akin to those found on the integer quantum Hall effect [37]. Regarding the scattering of spin waves in 3D systems, it was shown that the effective field generated by Bloch points on SWs resembles the magnetic field of the exotic Dirac monopole [38] in such a way that a Bloch point induces a nontrivial structure on the behavior of the SW phases [39].

This Letter focuses on SWs propagating through a magnetic hopfion. Using numerical and analytical calculations, we observe the appearance of a lenslike effect when the SWs reach the hopfion through its symmetry axis. However, if the SWs are incident on the plane perpendicular to the symmetry axis, we observe the Aharonov-Bohm effect. These results provide new ways to detect and manipulate magnetic hopfions, creating a bridge between the buoyant magnetic field of magnonics [40–44] and the creation, detection, and control of solitonic textures.

Structure of magnetic hopfions.—We consider a chiral magnetic system described by a micromagnetic energy functional $\mathcal{E}=\mathcal{E}_{\text{bulk}}+\mathcal{E}_{\text{PMA}}$, where $\mathcal{E}_{\text{bulk}}=\int_V \left[J(\mathfrak{D}_\mu \boldsymbol{n})^2/2-B_z n_z+K_{\text{bulk}}(1-n_z^2)\right] d^3\boldsymbol{r}$. Here, $\boldsymbol{n}$ is the normalized magnetization, $\boldsymbol{B}=B_z\boldsymbol{z}$ is the external magnetic field along the z axis, and $\mathfrak{D}_\mu=\partial_\mu+\kappa \boldsymbol{e}_\mu\times$ is the helical derivative [45], with $\boldsymbol{e}_\mu$ being a basis of the spatial coordinates, $\kappa=D/2J$ is the characteristic helical number, J is the exchange coupling [46], and D is the strength of the bulk Dzyaloshinskii-Moriya interaction characteristic for noncentrosymmetric materials. Previous works have demonstrated that hopfions are stable under different conditions [26–28,48]. In particular, a theoretical proposition considers local anisotropies at the upper and bottom layers of a cylindrical chiral nanomagnet, preventing the formation of 3D skyrmion tubes [31]. In this Letter, we follow this proposal, and include a second contribution to the energy functional consisting of a perpendicular magnetic anisotropy (PMA), given by $\mathcal{E}_{\text{PMA}}=K_S\int_S(1-\boldsymbol{n}_z^2)d^2\boldsymbol{r}$, where the second integral runs over the top and bottom surfaces of the magnetic system and K_S represents the PMA strength.

The formal description of a hopfion [48] can be given in terms of the $\mathfrak{su}(2)$ algebra, which works out as a representation of the rotation group $SO(3)$. That is, any element $\boldsymbol{\mathcal{R}}=\mathcal{R}_0\mathbb{I}_2+i\sum_\mu \mathcal{R}^\mu\hat{\sigma}_\mu$, where $\hat{\sigma}_\mu$ stands for the μth Pauli spin matrix ($\mu=1,2,3$). It can be noticed that these elements satisfy the relation $\mathcal{R}_0^2+\sum_\mu \mathcal{R}^\mu\mathcal{R}_\mu=1$ and generate a rotation operator with the group action $\hat{\boldsymbol{z}}\to\hat{\boldsymbol{n}}=\boldsymbol{\mathcal{R}}^{-1}\hat{\sigma}_z\boldsymbol{\mathcal{R}}$, where $\hat{\boldsymbol{n}}$ stands for $\sum_\mu n^\mu\hat{\sigma}_\mu$. The field of toroidal hopfions, $\boldsymbol{n}_H$, are constructed from a rotational symmetry texture $\boldsymbol{\mathcal{R}}_H(\boldsymbol{r})=e^{if(r)\hat{\boldsymbol{r}}/r}$, where the function $f(r)$ is smooth, monotonic, and satisfies $f(0)=0$ and $f(\infty)=\pi$ [23,49,50].

A hopfion can be characterized by its toroidal and poloidal cycles p, q, defined as the 2D-winding numbers on the (y,z) and (x,z) planes, respectively. A (p,q) hopfion, in spherical coordinates (r,θ,ϕ), can be described as

$$\begin{pmatrix} n_x \pm i n_y \\ n_z \end{pmatrix} = \begin{pmatrix} \sin(2\chi)e^{\pm i(q\phi-p\Theta+\gamma)} \\ \cos(2\chi) \end{pmatrix}, \tag{1}$$

where $\Theta(r,\theta)=\tan^{-1}\{\tan[f(r)]\cos(\theta)\}$ and $\chi(r,\theta)=\sin^{-1}\{\sin[f(r)]\sin(\theta)\}$. The parameter γ accounts for the helicity ($\gamma=0$ for Néel and $\gamma=\pi/2$ for Bloch type hopfions). An illustration of a hopfion and its magnetization profiles along the xy and xz planes parametrized by Eq. (1) for $\gamma=\pi/2$ are shown in Fig. 1, where white arrows represent the magnetization field.

Associated with a magnetic texture, there is a magnetic field defined by the Berry curvature $\boldsymbol{B}_\mu^{\text{em}}=\epsilon_{\mu\nu\eta}\boldsymbol{n}\cdot(\partial_\mu\boldsymbol{n}\times\partial_\nu\boldsymbol{n})$. In terms of this field, the Hopf index can be written as $\mathcal{Q}_H=(4\pi)^{-2}\int_V \boldsymbol{B}^{\text{em}}\cdot\boldsymbol{A}^{\text{em}}d\boldsymbol{r}$, where $\boldsymbol{B}^{\text{em}}=\nabla\times\boldsymbol{A}^{\text{em}}$. A remarkable property of hopfions is their vanishing global gyrovector $\boldsymbol{G}_H=\int_V \boldsymbol{B}^{\text{em}}d\boldsymbol{r}=\boldsymbol{0}$, indicating the absence of the Hall effect in the hopfion dynamics in the rigid body approximation [51].

Numerical simulations.—Using the GPU-accelerated MuMAX^3 package [52], we simulate a spin wave-hopfion system. Such code solves the Landau-Lifshitz-Gilbert equation [53,54] to emulate the magnetization dynamics. We consider a rectangular grid of $200\times200\times40$ nm^3 with a cell size of $a=1$ nm and open boundary conditions. In addition, we use a saturation magnetization, $M_s=100$ kA/m, an exchange stiffness $A_{\text{ex}}=0.1$ pJ/m, and $D=0.05$ mJ/m^2. In addition, a Gilbert damping parameter $\alpha=0.01$, a surface anisotropy constant $K_S=0.5$ mJ/m^2, and a volumetric anisotropy $K_{\text{bulk}}=5$ kJ/m^3 define the material.

The system starts in a configuration described by Eq. (1) and relaxes toward a final state as a function of the external magnetic field. The hopfion stability occurs for magnetic fields $\boldsymbol{B}=B_{\text{ext}}\hat{\boldsymbol{z}}$ within the range of $B_{\text{ext}}<B_c=0.05$ T. Above this threshold, one observes a Bloch point pair formation, also known as a toron state [55]. Therefore, from now on, we consider a magnetic field $B=0.025$ T for our calculations.

After stabilizing the magnetic hopfion, we study the behavior of SWs propagating along different directions with respect to the hopfion symmetry axis. The SW train is obtained by applying an ac magnetic field $\boldsymbol{B}_{\text{ac}}(t)=B_{\text{ac}}\cos(2\pi f_{\text{ac}}t)\hat{\boldsymbol{x}}$, with frequency $f_{\text{ac}}=60$ GHz and strength $B_{\text{ac}}=0.05$ T. The frequency was chosen just above the threshold required to display the effects of the

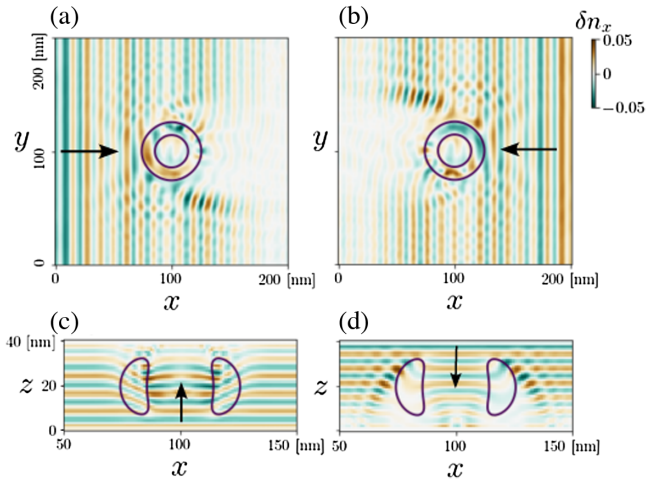

FIG. 2. Representation of the SW scattering by a hopfion obtained from micromagnetic simulations. The panels (a) and (b), and (c) and (d) depict the spatial oscillation $\delta n_x(\boldsymbol{r},t) = n_x(\boldsymbol{r},t) - n_x(\boldsymbol{r},0)$ on the (x,y) and (x,z) cross sections of the hopfion, respectively. Here, the black contours enclose the hopfion isosurface. The spin wave source is in the planes (a), $x = 0$; (b), $x = 200$ (nm); (c), $z = 0$; and (d), $z = 40$ (nm).

magnon scattering. This choice implies a magnon wavelength smaller than the hopfion length scale and larger than the cell size.

Our results are presented in Fig. 2, evidencing two phenomena. If the SWs propagate through the plane perpendicular to the hopfion symmetry axis, they act as a source of skew-scattering associated with a magnon Hall effect. In this case, the SWs' direction after crossing the hopfion depends on the propagation direction, as shown in Figs. 2(a) and 2(b). On the other hand, when the SWs propagate along the hopfion symmetry axis, a lenslike effect is observed. Depending on their propagation direction, after crossing the hopfion, SWs converge, as shown in Fig. 2(c), or diverge, as depicted in Fig. 2(d).

Analytical model.—To understand the behavior described above, we perform a theoretical analysis of the SWs, considering them as a small perturbation around the hopfion background field $\hat{\boldsymbol{n}}_H = \mathcal{R}^{-1}(\boldsymbol{r})\hat{\boldsymbol{z}}\mathcal{R}(\boldsymbol{r})$. The spin connection associated with this gauge transformation is defined by $\boldsymbol{\mathcal{A}}_\mu = \mathcal{R}^{-1}\mathfrak{D}_\mu\mathcal{R} = \mathcal{R}^{-1}\partial_\mu\mathcal{R} + \kappa\boldsymbol{e}_\mu$ [see Eq. (2) in Supplemental Material [56]]. Now, we excite the system using the Holstein-Primakoff transformation, or equivalently, linearizing $\hat{\boldsymbol{z}} \to \hat{\boldsymbol{z}}' \approx \psi\hat{\sigma}_+ + \psi^*\hat{\sigma}_- + (1-2|\psi|^2)\hat{\sigma}_z$, with $\hat{\sigma}_\pm = \hat{\sigma}_x \pm i\hat{\sigma}_y$. Hence, expanding the energy functional up to second order in $\Psi = (\psi, \psi^*)^t$, and using the identity $\partial_\mu(\mathcal{R}^{-1}\hat{\boldsymbol{n}}_0\mathcal{R}) = \mathcal{R}^{-1}(\partial_\mu\hat{\boldsymbol{n}}_0 + [\boldsymbol{\mathcal{A}}_\mu, \hat{\boldsymbol{n}}_0])\mathcal{R}$, we write the energy of the SWs in the presence of a hopfion as $\mathcal{E}_{\mathrm{SW}}[\Psi] = J\int \Psi^\dagger(\boldsymbol{r})\mathcal{H}_{\mathrm{SW}}\Psi(\boldsymbol{r})d^3\boldsymbol{r}/2$;, with the Bogoliubov–de Gennes Hamiltonian given by

$$\mathcal{H}_{\mathrm{SW}} = \begin{pmatrix} [i\partial_\mu - \mathcal{A}^Z_\mu(\boldsymbol{r})]^2 + \mathcal{U}(\boldsymbol{r}) & \mathcal{V}(\boldsymbol{r}) \\ \mathcal{V}^*(\boldsymbol{r}) & [-i\partial_\mu - \mathcal{A}^Z_\mu(\boldsymbol{r})]^2 + \mathcal{U}^*(\boldsymbol{r}) \end{pmatrix}. \tag{2}$$

The corresponding potentials are obtained and presented in Eqs. (5) and (6) of the Supplemental Material [56]. The result presented in Eq. (2) shows that magnons interacting with a hopfion are under the action of an effective magnetic field, defined by the Berry curvature $\boldsymbol{B}^{\mathrm{eff}} = \nabla \times \boldsymbol{\mathcal{A}}^Z$, that affects their dynamics. For $\kappa \ll 1$, it coincides with the emergent magnetic field of the texture, $\boldsymbol{B}^{\mathrm{em}}$. Under these statements, the magnon spin current is determined by

$$\mathcal{J}_\mu = \Psi^\dagger(-i\sigma_z\partial_\mu + \mathcal{A}^Z_\mu)\Psi, \tag{3}$$

meaning that magnons are coupled to a hopfion through the z component of the spin connection $\boldsymbol{\mathcal{A}}_\mu$.

Spin-wave scattering.—We now analyze the effect of the effective magnetic field on the SWs through scattering experiments. A semiclassical approach results in a useful approximation for highly energetic magnons. Let us consider a SW $\psi(\boldsymbol{r},t) = e^{-i\omega t + \boldsymbol{k}\cdot\boldsymbol{r}}$ incoming from the $-\boldsymbol{k}$ direction. In a semiclassical approach, the motion equation reads $\dot{\boldsymbol{r}} = \boldsymbol{p}/m^*$, where $m^* = \hbar M_s/(2Ja^2\gamma_0)$ determines the magnon mass. A Lorentz force, arising from the effective magnetic field, dominates the momentum evolution $\dot{\boldsymbol{p}} = \boldsymbol{B}^{\mathrm{eff}}(\boldsymbol{r}) \times \dot{\boldsymbol{r}} - \boldsymbol{\nabla}\mathcal{U}(\boldsymbol{r})$, where $\mathcal{U}(\boldsymbol{r})$ relates with the potential vector [see Eq. (5) in Supplementary Material [56]).

Another way to describe the magnon scattering on a hopfion is by considering its finite toroidal moment, given by $\boldsymbol{t} = \int d^3r[\boldsymbol{r} \times \boldsymbol{B}^{\mathrm{eff}}(\boldsymbol{r})]/2 = \boldsymbol{t}_z\hat{\boldsymbol{z}}$. One can notice that the hopfion's toroidal moment points along the direction of its symmetry axis, and its magnitude is proportional to the total topological charge contained within the hopfion. Therefore, by using the Belavin-Polyakov ansatz, $\sin[f(r)] = 2rR_0/(r^2 + R_0^2)$, one obtains $\mathrm{t}_z = 3\pi^3 pR_0^2/2$. Here, R_0 stands for the lateral radius of the Hopfion, which can be estimated from the skyrmionlike structure arising at the xz plane. A direct effect of the toroidal magnetic moment appears by considering a wavefront propagating along the z axis. Magnons propagating with velocity $v_z\hat{\boldsymbol{z}}$, are subjected to a radial force $\boldsymbol{F}_\rho = 2p\sin^2(f)f'\sin(\theta)v_z\boldsymbol{\rho}/r$ [56]. Because of its explicit dependence on v_z, the effective force exerted by hopfions on magnons can be attractive or repulsive depending on the direction of the SWs' propagation. These radial forces are responsible for the lenslike effect previously obtained from micromagnetic simulations. Our calculations do not consider the full extent of the dipolar effects. Indeed, previous works have revealed that even including magnetostatic interactions, the emergent topological fields continue

playing a key role in magnon interferometry phenomena. This behavior has been confirmed in other systems, such as skyrmions [60] and Bloch points [61]. In our approach, the problem can be reduced to the SWs scattering on a system composed of two skyrmions with the same radius ($\approx R_0$) and opposite polarities and helicities [33,62]. Assuming that the effective magnetic flux is highly concentrated at the inner region of the torus isosurface, the magnon scattering can be considered as the intersection of the cyclotron orbit in that region. In this context, following a similar argument as in Ref. [63], the magnon deflection Hall angle is given by $\theta_{\mathrm{Hall}} \approx \pi/\rho_{\mathrm{cyc}}$, where $\rho_{\mathrm{cyc}} \approx m^* v R_0/4p$ is the cyclotron radius.

To complement our theoretical analysis, we make use of the KWANT package [58] to solve Eq. (2). KWANT consists of a Python library specialized in quantum transport. While its specific purpose is related to calculating the electronic properties of quantum systems, it is possible to use it in the context of generic wave propagation and obtain the scattering states of SWs. Using this package, we look for solutions with boundary conditions in the form of incoming plane waves from different directions. Our results evidence that when SWs propagate along the plane perpendicular to the hopfion's symmetry axes, a skew-scattering effect occurs with opposite SW propagation directions, either from left to right, as shown in Fig. 3(a) or from right to left, as illustrated in Fig. 3(b). On the other hand, when SWs propagate from bottom to top, the hopfion's effect is equivalent to what occurs with light crossing a divergent lens, as seen in Fig. 3(c). Waves propagating from top to bottom experience a convergent lenslike effect, as shown in Fig. 3(d). These results agree with our theoretical analysis, which predicts that the focal length of such a lenslike system depends on the toroidal moment of the hopfion. We highlight that a hopfion with an opposite toroidal moment would also produce an opposite convergent or divergent lenslike effect, depending on the SWs' incoming direction.

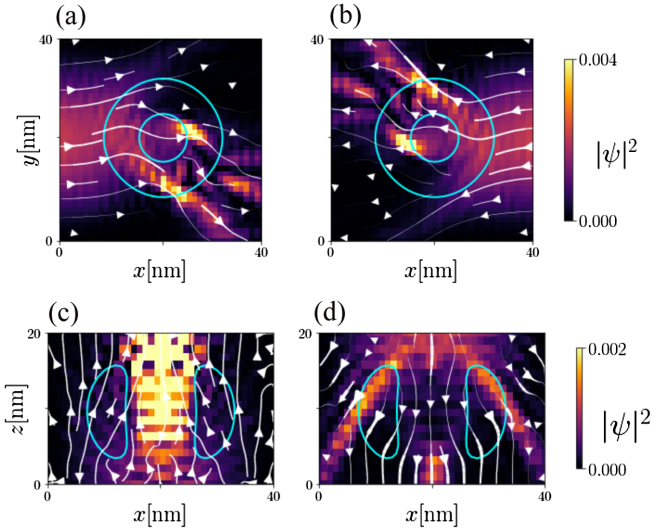

FIG. 3. Scattering states associated with incoming SWs obtained using the KWANT package. The lines correspond to streamlines of the magnon current in Eq. (3). Color intensity represents the magnon local density, $\rho = |\psi|^2$. Solid lines refer to the location of the hopfion. Panels (a) and (b) illustrate the skew-scattering of SWs propagating along the xy plane. (c) and (d) show the SWs propagating parallel to the hopfion's symmetry axes.

Finally, a magnon Ahronov-Bohm effect arises from the effective flux piercing each plane at the cross section of the system. It acquires a simple form in the xy plane where the phase difference between two interfering arbitrary magnon paths enclosing the hopfion can be calculated considering the integral of the potential vector $\Phi_{\mathrm{flux}} = \oint \boldsymbol{A} \cdot \boldsymbol{dr}$ over a circle of radius much larger than the system size. From the adopted model, we find that the net flux $\Phi_{\mathrm{flux}} = 2\kappa R_0$, which is twice the flux for one skyrmion [57]. This flux opens up the possibility of magnon interference experiments [39] that could be used to detect the presence of a hopfion.

Discussion.—This Letter presents an analysis of SWs propagating across a hopfion texture using micromagnetic simulations and an analytical model. The natural way the hopfion affects the propagation of linear excitations is through Berry's phases that depend on the geometrical details of the hopfion. This behavior can be understood as an effective magnetic field that acts on the SWs. Using micromagnetic and analytical calculations and assuming a short wavelength, we observe two different regimes. First, there is a lenslike effect for SWs propagating along the symmetry axis of the hopfion. This effect can be relevant for controlling magnonic devices [64]. The focal length of such an effective magnonic lens depends on the toroidal moment of the hopfion. The second effect occurs when SWs propagate through the plane perpendicular to the symmetry axis. In this case, the hopfion acts as a source of skew-scattering, leading to a magnon Hall effect. Therefore, we have shown that the propagation of SWs is sensitive to the relative plane through which the propagation takes place.

Because of the hopfion magnetic structure, the magnonic signature is anisotropic. That is, it depends on the incoming SWs' direction. This direction-dependent response does not commonly occur for other magnetic textures such as skyrmions and Bloch points. The lenslike behavior does not occur in other magnetic textures, since it comes from the toroidal moment of the hopfion. These results indicate that hopfions should serve as a platform to implement magnonic holographic devices suitable for data processing [65]. The latter notion consists of imaging magnetization textures exploiting interference of SWs crossing them, following their optical holography counterparts. Magnon holography has some drawbacks, such as the fact that spin waves cannot match the propagation speed of photons and suffer from higher losses. Nevertheless, they offer better compatibility with electronic systems at the nanometric

scale, opening up the potential for constructing high-density magnonic holograms [65]. However, the field of magnonic imaging is still in its early stages, and several challenges in both physical and technological aspects need to be addressed before its practical use can be fully realized.

Funding is acknowledged from Fondecyt Regular No. 1230515, No. 1230747, and No. 1220215, and Financiamiento Basal para Centros Científicos y Tecnológicos de Excelencia AFB220001. C. S. thanks the financial support provided by ANID National Doctoral Scholarship No. 21210450. V. L. C.-S. acknowledges the support of the INCT of Spintronics and Advanced Magnetic Nanostructures (INCT-SpinNanoMag), the Brazilian agencies CNPq (Grants No. 305256/2022-0 and No. 406836/2022-1) and Fapemig (Grant No. APQ-00648-22).

[1] R. Rajaraman, *Solitons and Instantons: Volume 15*, North-Holland Personal Library (North-Holland, Oxford, England, 1987).
[2] N. D. Mermin, Rev. Mod. Phys. **51**, 591 (1979).
[3] M. Remoissenet, *Waves Called Solitons*, 3rd ed., Advanced Texts in Physics (Springer, Berlin, Germany, 1999).
[4] G. E. Brown and M. Rho, *Multifaceted Skyrmion, The*, edited by G. E. Brown and M. Rho (World Scientific Publishing, Singapore, 2010).
[5] T. Skyrme, Nucl. Phys. **31**, 556 (1962).
[6] S. S. P. Parkin, M. Hayashi, and L. Thomas, Science **320**, 190 (2008).
[7] P. Dey and J. N. Roy, *Spintronics* (Springer, Singapore, 2021), 10.1007/978-981-16-0069-2.
[8] Q. Wang, Y. Zeng, K. Yuan, Q. Zeng, P. Gu, X. Xu, H. Wang, Z. Han, K. Nomura, W. Wang, E. Liu, Y. Hou, and Y. Ye, Natl. Electron. Rev. **6**, 119 (2023).
[9] P. Landeros and Á. S. Núñez, J. Appl. Phys. **108**, 033917 (2010).
[10] C. Ulloa and A. S. Nunez, Phys. Rev. B **93**, 134429 (2016).
[11] S. Muhlbauer, B. Binz, F. Jonietz, C. Pfleiderer, A. Rosch, A. Neubauer, R. Georgii, and P. Boni, Science **323**, 915 (2009).
[12] A. Fert, N. Reyren, and V. Cros, Nat. Rev. Mater. **2**, 17031 (2017).
[13] M. Schott, A. Bernand-Mantel, L. Ranno, S. Pizzini, J. Vogel, H. Béa, C. Baraduc, S. Auffret, G. Gaudin, and D. Givord, Nano Lett. **17**, 3006 (2017).
[14] K. Huang, D.-F. Shao, and E. Y. Tsymbal, Nano Lett. **22**, 3349 (2022).
[15] W. Du, K. Dou, Z. He, Y. Dai, B. Huang, and Y. Ma, Nano Lett. **22**, 3440 (2022).
[16] W. Wang, D. Song, W. Wei, P. Nan, S. Zhang, B. Ge, M. Tian, J. Zang, and H. Du, Nat. Commun. **13**, 1593 (2022).
[17] D. Chakrabartty, S. Jamaluddin, S. K. Manna, and A. K. Nayak, Commun. Phys. **5**, 189 (2022).
[18] A. Fernández-Pacheco, R. Streubel, O. Fruchart, R. Hertel, P. Fischer, and R. P. Cowburn, Nat. Commun. **8**, 15756 (2017).
[19] C. Donnelly, M. Guizar-Sicairos, V. Scagnoli, M. Holler, T. Huthwelker, A. Menzel, I. Vartiainen, E. Müller, E. Kirk, S. Gliga, J. Raabe, and L. J. Heyderman, Phys. Rev. Lett. **114**, 115501 (2015).
[20] D. Makarov, O. M. Volkov, A. Kákay, O. V. Pylypovskyi, B. Budinská, and O. V. Dobrovolskiy, Nat. Commun. **2022**, 2101758 (2021).
[21] D. Sanz-Hernández, A. Hierro-Rodriguez, C. Donnelly, J. Pablo-Navarro, A. Sorrentino, E. Pereiro, C. Magén, S. McVitie, J. M. de Teresa, S. Ferrer, P. Fischer, and A. Fernández-Pacheco, ACS Nano **14**, 8084 (2020).
[22] L. Faddeev and A. J. Niemi, Nature (London) **387**, 58 (1997).
[23] A. Kosevich, B. Ivanov, and A. Kovalev, Phys. Rep. **194**, 117 (1990).
[24] P. Sutcliffe, J. Phys. A **51**, 375401 (2018).
[25] Y. Liu, H. Watanabe, and N. Nagaosa, Phys. Rev. Lett. **129**, 267201 (2022).
[26] F. N. Rybakov, N. S. Kiselev, A. B. Borisov, L. Döring, C. Melcher, and S. Blügel, APL Mater. **10**, 111113 (2022).
[27] S. Castillo-Sepúlveda, R. Cacilhas, V. L. Carvalho-Santos, R. M. Corona, and D. Altbir, Phys. Rev. B **104**, 184406 (2021).
[28] R. M. Corona, E. Saavedra, S. Castillo-Sepúlveda, J. Escrig, D. Altbir, and V. L. Carvalho-Santos, Nanotechnology **34**, 165702 (2023).
[29] N. Kent, N. Reynolds, D. Raftrey, I. T. G. Campbell, S. Virasawmy, S. Dhuey, R. V. Chopdekar, A. Hierro-Rodriguez, A. Sorrentino, E. Pereiro, S. Ferrer, F. Hellman, P. Sutcliffe, and P. Fischer, Nat. Commun. **12**, 1562 (2021).
[30] X. S. Wang, A. Qaiumzadeh, and A. Brataas, Phys. Rev. Lett. **123**, 147203 (2019).
[31] B. Gobel, I. Mertig, and O. A. Tretiakov, Phys. Rep. **895**, 1 (2021).
[32] Z. Zhang, K. Lin, Y. Zhang, A. Bournel, K. Xia, M. Kläui, and W. Zhao, Sci. Adv. **9**, eade7439 (2023).
[33] Y. Shen, B. Yu, H. Wu, C. Li, Z. Zhu, and A. V. Zayats, Adv. Opt. Photonics **5**, 015001 (2023).
[34] H. Yu, J. Xiao, and H. Schultheiss, Phys. Rep. **905**, 1 (2021).
[35] J. Lan and J. Xiao, Phys. Rev. B **106**, L020404 (2022).
[36] K. A. van Hoogdalem, Y. Tserkovnyak, and D. Loss, Phys. Rev. B **87**, 024402 (2013).
[37] A. Roldán-Molina, A. S. Nunez, and J. Fernández-Rossier, New J. Phys. **18**, 045015 (2016).
[38] R. G. Elías, V. L. Carvalho-Santos, A. S. Núñez, and A. D. Verga, Phys. Rev. B **90**, 224414 (2014).
[39] V. Carvalho-Santos, R. Elías, and A. S. Nunez, Ann. Phys. (Amsterdam) **363**, 364 (2015).
[40] P. Pirro, V. I. Vasyuchka, A. A. Serga, and B. Hillebrands, Nat. Rev. Mater. **6**, 1114 (2021).
[41] H. Yuan, Y. Cao, A. Kamra, R. A. Duine, and P. Yan, Phys. Rep. **965**, 1 (2022).
[42] B. Zare Rameshti, S. Viola Kusminskiy, J. A. Haigh, K. Usami, D. Lachance-Quirion, Y. Nakamura, C.-M. Hu, H. X. Tang, G. E. Bauer, and Y. M. Blanter, Phys. Rep. **979**, 1 (2022).
[43] Z.-Q. Wang, Y.-P. Wang, J. Yao, R.-C. Shen, W.-J. Wu, J. Qian, J. Li, S.-Y. Zhu, and J. Q. You, Nat. Commun. **13**, 7580 (2022).

[44] A. Roldán-Molina, A. S. Nunez, and R. A. Duine, Phys. Rev. Lett. **118**, 061301 (2017).
[45] C. Melcher, Proc. R. Soc. A **470**, 20140394 (2014).
[46] Here, following the ideas of Jin *et al.* [47] that analyze the magnon-driven dynamics of skyrmions, we assume that the next-nearest neighbors corrections to the exchange energy, that in the continuum limit is $\mathcal{E}^{\mathrm{ex}}_{\mathrm{nnn}} = C^{\mu\nu}\int \partial^2_\mu \boldsymbol{n}\cdot\partial^2_\nu \boldsymbol{n} d^3\boldsymbol{r}$, with $C^{\mu\nu}$ corresponding to the respective coupling constant, is negligible in the spin wave Hamiltonian interacting with the hopfion. Therefore, the Heisenberg exchange dominates the interaction, that is, $\mathcal{E}^{\mathrm{ex}}_{\mathrm{nnn}} \ll \mathcal{E}_{\mathrm{bulk}}$.
[47] Z. Jin, T. T. Liu, Y. Liu, Z. P. Hou, D. Y. Chen, Z. Fan, M. Zeng, X. B. Lu, X. S. Gao, M. H. Qin, and J.-M. Liu, New J. Phys. **24**, 073047 (2022).
[48] J.-S. B. Tai and I. I. Smalyukh, Phys. Rev. Lett. **121**, 187201 (2018).
[49] R. Zarzuela, H. Ochoa, and Y. Tserkovnyak, Phys. Rev. B **100**, 054426 (2019).
[50] Three-dimensional magnetic solitons classified under the third homotopy group is characterized by the Hopf index $\mathcal{Q}_H$ of the texture that quantifies the linking structure of the magnetization. The Hopf index is formally defined as $\mathcal{Q}_H = (1/8\pi^2)\int_V \varepsilon_{ijk}\varepsilon_{\alpha\beta\gamma\delta}\mathcal{R}_\alpha(\partial\mathcal{R}_\beta/\partial x_i)(\partial\mathcal{R}_\gamma/\partial x_j)(\partial\mathcal{R}_\delta/\partial x_k)d\boldsymbol{x}$, where Einstein convention is assumed for repeated indices. In particular, for the toroidal hopfion represented by $\boldsymbol{\mathcal{R}}_H$, we obtain $\mathcal{Q}_H = 1$.
[51] Y. Liu, W. Hou, X. Han, and J. Zhang, Phys. Rev. Lett. **124**, 127204 (2020).
[52] A. Vansteenkiste, J. Leliaert, M. Dvornik, M. Helsen, F. Garcia-Sanchez, and B. V. Waeyenberge, AIP Adv. **4**, 107133 (2014).
[53] L. Landau and E. Lifshits, Ukr. J. Phys. **53**, 14 (2008), https://verga.cpt.univ-mrs.fr/pdfs/Landau-1935fk.pdf.
[54] T. L. Gilbert, IEEE Trans. Magn. **40**, 3443 (2004).
[55] L. Bo, L. Ji, C. Hu, R. Zhao, Y. Li, J. Zhang, and X. Zhang, Appl. Phys. Lett. **119**, 212408 (2021).
[56] See Supplemental Material at http://link.aps.org/supplemental/10.1103/PhysRevLett.131.166702 for further details, which includes Refs. [57–59].
[57] J. H. Han, *Skyrmions in Condensed Matter* (Springer International Publishing, New York, 2017), 10.1007/978-3-319-69246-3.
[58] Christoph W. Groth, Michael Wimmer, Anton R. Akhmerov, and Xavier Waintal, New J. Phys. **16**, 063065 (2014).
[59] Sergey S. Pershoguba, Domenico Andreoli, and Jiadong Zang, Phys. Rev. B **104**, 075102 (2021).
[60] C. Back, V. Cros, H. Ebert, K. Everschor-Sitte, A. Fert, M. Garst, T. Ma, S. Mankovsky, T. L. Monchesky, M. Mostovoy, N. Nagaosa, S. S. P. Parkin, C. Pfleiderer, N. Reyren, A. Rosch, Y. Taguchi, Y. Tokura, K. von Bergmann, and J. Zang, J. Phys. D **53**, 363001 (2020).
[61] A. Tapia, C. Saji, A. Roldan, and A. S. Nunez, arXiv: 305.18704v1.
[62] N. Nagaosa and Y. Tokura, Nat. Nanotechnol. **8**, 899 (2013).
[63] M. W. Daniels, W. Yu, R. Cheng, J. Xiao, and D. Xiao, Phys. Rev. B **99**, 224433 (2019).
[64] Z. Wang, Z.-X. Li, R. Wang, B. Liu, H. Meng, Y. Cao, and P. Yan, Appl. Phys. Lett. **117**, 222406 (2020).
[65] A. Khitun, J. Appl. Phys. **113**, 164503 (2013).